Binding of 2,6- and 2,7-Dihydroxynaphthalene to Wild-Type and E-B13Q Insulins: Dynamic, Equilibrium, and Molecular Modeling Investigations†

Curtis R. Bloom,‡,§ Robert Heymann,‡ Niels C. Kaarsholm,|| and Michael F. Dunn*,‡

Department of Biochemistry, University of California, Riverside, Riverside, California 92521, and Novo Research Institute, Novo Nordisk A/S, DK-2880 Bagsvaerd, Denmark

Received April 1, 1997; Revised Manuscript Received July 16, 1997⊗

ABSTRACT: The binding of phenolic ligands to the insulin hexamer occurs as a cooperative allosteric process. Investigations of the allosteric mechanism from this laboratory resulted in the postulation of a model consisting of a three-state conformational equilibrium and the derivation of a mathematical expression to describe the insulin system. The proposed mechanism involves allosteric transitions among two states of high symmetry, designated T_3T_3' (a low affinity state) and R_3R_3' (a high affinity state), and a third state of lower symmetry, designated $T_3^oR_3^o$ (a state of mixed low and high affinities). To further characterize this mechanism, we present rapid kinetic fluorescence studies, equilibrium binding isotherms, and molecular modeling investigations for the Co(II)-substituted wild-type and E-B13Q mutant hexamers. These studies show that the measured on and off rates (k_{on} and k_{off}) for the binding of the allosteric ligands 2,6- and 2,7-dihydroxynaphthalene provide an independent measure of the dissociation constant for binding to the $T_3^oR_3^o$ conformation (K_R^o). These constants are in agreement with the value obtained by computer fitting of the equilibrium binding isotherms to the quantitative allosteric mechanism. We analyze the structural differences between the $T_3^oR_3^o$ and R_6 phenolic binding sites and predict the structures of the $T_3^oR_3^o$−2,6-DHN and R_6−2,6-DHN complexes by 3-D molecular modeling. Assignment of H-bonding of the first hydroxyl group to CysA6 and CysA11 has been supported by stacking interactions analogous to phenol using ^{1}H-NMR. H-bonding of the second hydroxyl group of 2,6-DHN to the GluB13 carboxylate side chains is predicted by molecular modeling and is supported by a reduction of affinity for Ca^{2+}, which is postulated to bind to the GluB13 side chains.

The binding of phenol to the insulin hexamer has become a valuable tool for the study of allostery and cooperativity in ligand binding processes (Kaarsholm et al., 1989; Roy et al., 1989; Brader et al., 1991; Brzovic et al., 1994; Bloom et al., 1995). In 1989, phenol was found to bind to a pocket located on the interface between adjacent dimers in the R_6 hexamer[1] (Derewenda et al., 1989). Phenol binding can increase the stability of the hexamer by a factor $>1 \times 10^6$ (Rahuel-Clermont et al., 1997). Crystallographic analysis of the hexamer alone (the T_6-state) (Blundell et al., 1972; Baker et al., 1988), in the presence of high concentrations of strong electron-donating anions (the $T_3^oR_3^o$ state) (Smith et al., 1984; Ciszak and Smith, 1994; Whittingham et al., 1995) or high concentrations of phenol (the R_6 state) (Derewenda et al., 1989), reveals significant structural changes (compare parts A and B of Figure 1). Ligand binding assays demonstrated that the T- to R-state transition of the hexamer is a cooperative process (Brader et al., 1991; Choi et al., 1993; Brzovic et al., 1994; Bloom et al., 1995). Substitution of Co^{2+} for the naturally occurring Zn^{2+} ion provides a spectroscopic probe of the ligand-mediated conformational change.[2] Using this probe, several compounds related to phenol have been discovered which bind to the R-state with various affinities (Roy et al., 1989; Brader et al., 1991; Choi et al., 1993; Brzovic et al., 1994; Bloom et al., 1995). To date, the highest affinity phenolic-type ligands identified are resorcinol, 2,6- and 2,7-dihydroxynaphthalene, and 7-hydroxyindole (Bloom et al., 1995; Dodson et al., 1993).

In the absence of phenolic ligands and certain anionic ligands, the hexamer exists primarily in the T_6 conformation, a species which possesses one 3-fold[3] and three pseudo-2-fold axes of symmetry (Figure 1A) (Baker et al., 1988). Residues B1 through B9 form an extended conformation; this structure is followed by an α-helical segment from B10 to B19. Within each dimer, residues B24 to B26 form an antiparallel β-sheet with the same residues from the adjacent monomer. Two identical Zn^{2+} binding sites are formed in

† This work was supported by a gift from the Novo Research Institute.

* To whom correspondence should be addressed.

‡ University of California, Riverside.

§ Current address: Department of Chemistry, California Institute of Technology, Pasadena, CA.

|| Novo Research Institute.

⊗ Abstract published in *Advance ACS Abstracts,* October 1, 1997.

[1] The global conformations of insulin hexamer forms with extended (T) and α-helical (R) conformations of B-chain residues 1−8 are designated as T_6, T_3R_3, and R_6 (Kaarsholm et al., 1989). T_3T_3' and R_3R_3' designate conformations with one 3-fold axis and three pseudo-2-fold axes of symmetry, while $T_3^oR_3^o$ designates the hexamer with only a single, 3-fold, axis of symmetry (Bloom et al., 1995). Abbreviations: KNF, the sequential model for allostery (Koshland et al., 1966); SMB, the half-site reactivity (suboptimal symmetry) model for cooperativity (Seydoux et al., 1974); MWC, the concerted (symmetry conserved) model for positive cooperativity (Monod et al., 1965); L_o^A and L_o^B, allosteric constants for the interconversion of T_3T_3' with $T_3^oR_3^o$ and $T_3^oR_3^o$ with R_3R_3', respectively; K_R^o, K_R, and K_R', dissociation constants for ligand binding to the phenolic pockets of the R_3^o, R_3, and R_3' units of $T_3^oR_3^o$ and R_3R_3', respectively; K_T, dissociation constant for the binding of phenolic ligands to trimeric units in the T-state conformation; $K_D = k_{off}/k_{on} = k_{-1}/k_1$; ρ, fraction of R-state species; ^{1}H-NMR, proton nuclear magnetic resonance; 2,6- and 2,7-DHN, 2,6- and 2,7-dihydroxynaphthalene, respectively; PABA, *p*-aminobenzoic acid.

S0006-2960(97)00761-7 CCC: $14.00

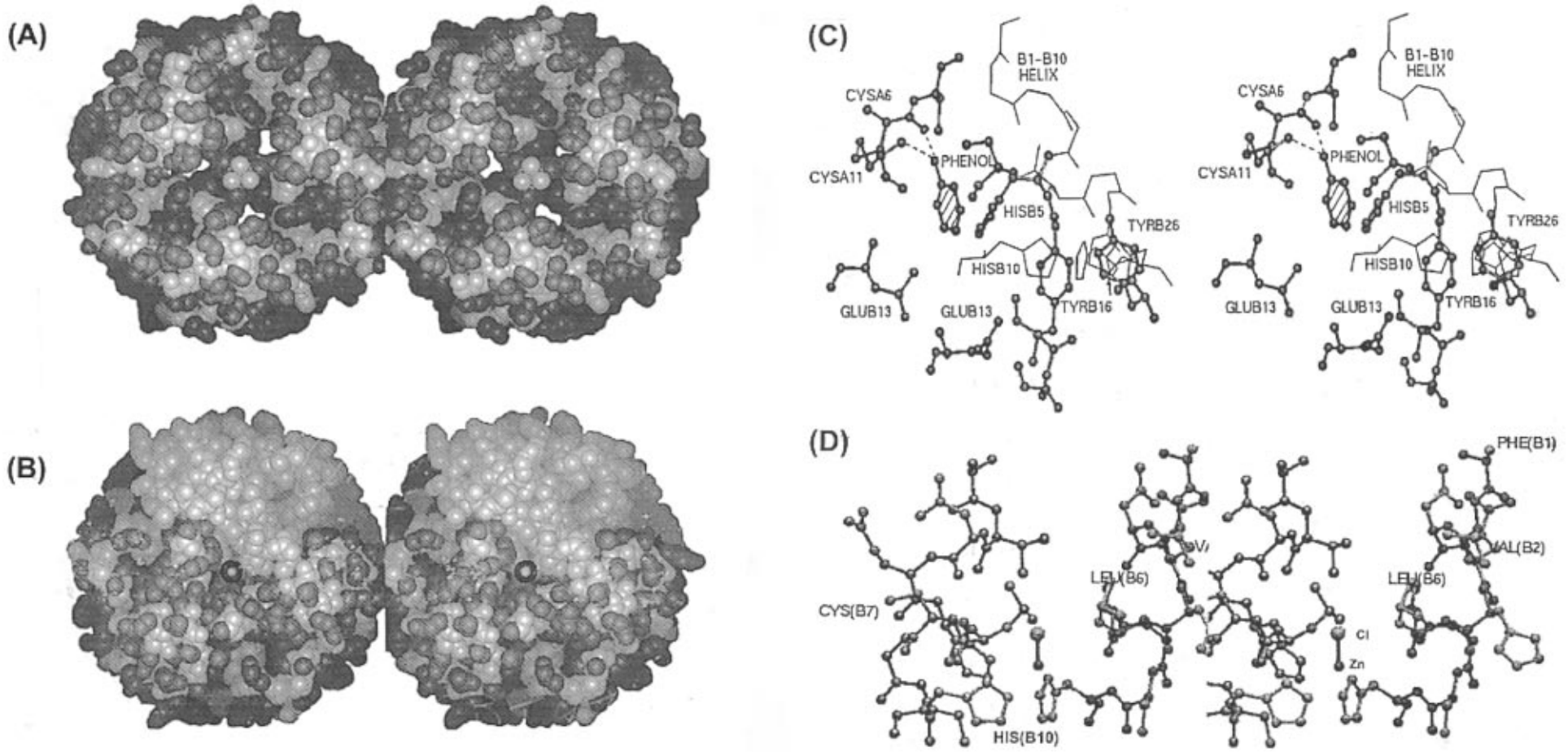

FIGURE 1: Stereo diagrams depicting the structure of the insulin hexamer. (A) Space-filling model of T_6 viewed along the 3-fold symmetry axis. Side chain atoms are shown as dark spheres, and main chain atoms are shown as lighter spheres. The three water molecules coordinated to the HisB10 zinc ion are shown at the center of the hexamer. The three water-filled channels which extend through the hexamer parallel to the 3-fold axis are shown empty. The coordinates used were taken from the Brookhaven Protein Data Bank for pig insulin (Baker et al., 1998). (B) Space-filling model of the R_6−phenol complex with chloride coordinated to the HisB10 sites viewed along the 3-fold symmetry axis. The conversion of residues B1−9 from the extended conformation of the T-state to the α-helical conformation of the R-state creates a three-helix bundle about the 3-fold symmetry axis and generates the narrow tunnel down to the HisB10 site. One dimeric unit (top) is shown as light spheres. The other two dimeric units are shown with the side chain atoms as dark spheres and the main chain atoms as light spheres. The chloride ion coordinated to the HisB10 zinc ion is positioned at the center of the hexamer on the 3-fold symmetry axis. The bound phenols are completely buried and therefore can not be seen in this space-filling model. Coordinates provided by G. David Smith. (C) Ball and stick stereo diagram of phenol (striped ring) bound to a phenolic pocket of the R_6 hexamer. H-bonding interactions between the hydroxyl group of phenol and backbone residues CysA11 and CysA6 are depicted by dashed lines. The aromatic ring of phenol makes van der Waals contact with the ring of HisB5 which makes contact with TyrB16, and TyrB16 makes contact with TyrB26. Phenol only partially fills the pocket. The bottom of the pocket is capped by two GluB13 residues. The phenolic pocket is about 8 Å distant from the HisB10 site (right background). Diagram redrawn from Rahuel-Clermont et al. (1997) with permission. (D) Ball and stick stereo diagram of the R_6 HisB10 site of the chloride complex viewed perpendicular to the 3-fold axis with one dimeric unit cut away to reveal the zinc ion site and the tunnel. Zn^{2+} and Cl^- are shown bonded to each other. The tunnel extends from the metal ion to the surface of the protein (top) along the 3-fold axis which passes through Zn^{2+} and Cl^-. Redrawn from Choi (1994) with permission. Coordinates provided by G. David Smith.

shallow depressions at both ends of the 3-fold axis of symmetry with octahedral ligand fields, each involving three HisB10 imidazolyl rings and three water molecules (Figure 1A). A single Ca^{2+} ion binds in the vicinity of the hexamer center (Sudmeier et al., 1981). X-ray diffraction studies of the Cd^{2+} and Pb^{2+} complexes (Hill et al., 1991) indicate three equivalent sites each exhibiting one-third occupancy, and therefore each hexamer binds a single Ca^{2+} ion at this locus (Storm & Dunn, 1985). This unusual divalent metal ion binding site is comprised of three closely spaced, symmetry-related GluB13−GluB13 carboxylate pairs. Binding of Ca^{2+} is known to stabilize the formation of the hexamer, presumably by alleviating unfavorable charge−charge repulsions among the six carboxylate side chains (Kaarsholm et al., 1990).

In the T to R conformational transition, residues B1 through B9 coil to make a continuous α-helix from B1 to B19, relocating the ring of PheB1 by ∼30 Å (Derewenda et al., 1989; Brader et al., 1991; Smith & Dodson, 1992a,b; Brzovic et al., 1994). In the absence of phenolic ligands, strong electron donating anions such as SCN^-, N_3^-, CN^-, Cl^-, Br^-, and I^- can stabilize a mixed T- and R-state oligomer with a $T_3{}^oR_3{}^o$ conformation (Figure 2) (Kaarsholm et al., 1989; Brader et al., 1991; Brzovic et al., 1994; Whittingham et al., 1995; Choi et al., 1996). Due to the asymmetry of the T−R dimeric units, the hexamer retains a true 3-fold axis of symmetry[3] while losing the three pseudo-2-fold axes (Ciszak & Smith, 1994). The T-state monomers (Ludvigsen et al., 1994) retain the folding motif of subunits in the T_6 hexamer. In the R_3 units of R_6 and $T_3{}^oR_3{}^o$, the new helical segments are arranged about the 3-fold axis creating narrow, 12 Å deep tunnels extending down to the Zn^{2+} site (Figure 1B,D) (Smith & Dodson, 1992a,b). The three water molecules found in the octahedral coordination sphere of the T-state sites (Figure 1A) are replaced by one exchangeable anionic ligand (Figure 1B,D), and the coordination is restricted to tetrahedral (or 5-coordinate with small bidentate anions) (Roy et al., 1989; Brader et al., 1991, 1997; Choi et al., 1993; Brzovic et al., 1994; Bloom et al., 1995). The coil-to-helix rearrangement of the B-chain creates a hydrophobic ligand binding site which extends from the center of the hexamer at GluB13 to just below the surface (Figure 1C) (Derewenda et al., 1989; Smith & Dodson, 1992a,b). Three identical pockets are formed in $T_3{}^oR_3{}^o$ (Ciszak & Smith, 1994; Whittingham et al., 1995), and six nearly identical pockets are formed in R_6 (Derewenda et al., 1989; Smith & Dodson, 1992a,b). These pockets are large enough to bind ligands such as phenol, cresol, or dihydroxynaphthalenes (Choi et al., 1993; Bloom et al., 1995) and herein are referred to as the phenolic pockets (Figure 1C).

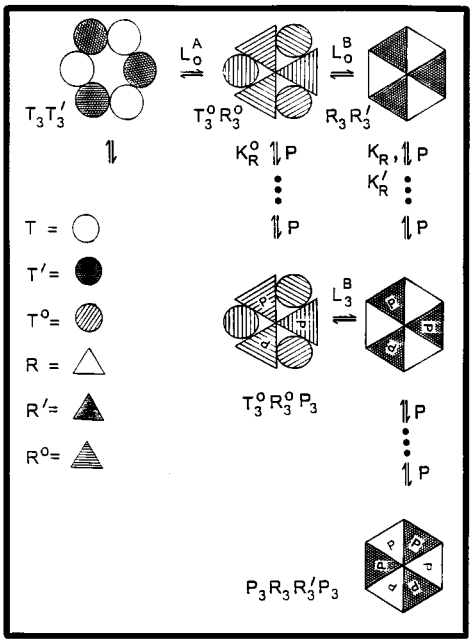

FIGURE 2: Complex equilibria for interconversion of the three conformation states T_3T_3', $T_3{}^oR_3{}^o$, and R_3R_3', coupled to ligand binding steps for each R-state conformation. $L_o{}^A$ and $L_o{}^B$ are the allosteric constants for the concerted transitions between T_3T_3' and $T_3{}^oR_3{}^o$ and between $T_3{}^oR_3{}^o$ and R_3R_3'. For the sake of brevity, the allosteric transitions $L_1{}^B$ and $L_2{}^B$ (analogous to $L_3{}^B$) for the interconversion of liganded states are not shown. The dots represent the binding equilibria for the formation of $T_3{}^oR_3{}^oP$ and $T_3{}^oR_3{}^oP_2$ and for the formation of the various ligation states R_3R_3' through $P_3R_3R_3'P_3$. $K_R{}^o$, K_R, and K_R' are the dissociation constants for binding to the phenolic pockets of $T_3{}^oR_3{}^o$ and of the R_3 and R_3' units of R_3R_3', respectively. Reproduced from Brzovic et al. (1994) with permission.

The phenolic pockets of R_6 (Smith & Dodson 1992a,b; coordinates provided by David Smith) are similar but not identical in shape to those found in $T_3{}^oR_3{}^o$ (Derewenda et al., 1989; Ciszak & Smith, 1993; coordinates provided by David Smith). Each pocket is formed from adjacent subunits. Therefore, each of the three phenolic pockets of $T_3{}^oR_3{}^o$ is comprised of an R^o−R^o interface with contributions from a T^o−GluB13 side chain, while each of the six pockets of R_6 is comprised of an R−R interface (or R′−R′ interface; the prime designates the slight differences in R-state conformations of the R_6 hexamer due to pairwise asymmetry) and carboxylates from an R′−GluB13 (or R−GluB13) (Figure 1C).

Recent studies have revealed that the T- to R-state transition of the insulin hexamer exhibits both negative[4] and positive cooperative behavior involving two distinct conformational transitions (Brzovic et al., 1994; Bloom et al., 1995). The evidence for only three global conformational states (T_6,

[2] The structure of the T_3R_3 complex determined in the presence of 0.75 M Cl^- (Ciszak & Smith, 1994) shows disorder at the HisB10 site of the T_3 unit, indicating that, in this crystalline hexamer, the T_3 unit can form either a tetrahedral HisB10 site with the fourth position occupied by Cl^- or an octahedral site with three coordinated waters. The tetrahedral T_3 site appears to arise from a combination of factors: (a) a very high chloride ion concentration and (b) an electrostatic requirement of the bound zinc ion which can be satisfied either by three His side chains and three H_2O molecules or by three His and one chloride ion. Due to the coordination geometry plasticity of Zn(II), coordination number and geometry are dictated by steric and electronic interactions among the ligands and the need to satisfy the electrostatic charge on the metal center. The symmetry of the site then dictates that chloride bind on the 3-fold symmetry axis. Examination of the X-ray structures of T-state hexamers indicates that the large size of Cl^- (ionic radius ∼1.8 Å) would not allow formation of an octahedral complex, for example, with one chloride ion and two water molecules. The T_3 unit of the Zn(II)-substituted T_3R_3−SCN^- complex also gives a tetrahedral zinc site. In contrast, the Co(II)-substituted SCN^- complex gives a T_3R_3 species with SCN^- coordinated to a tetrahedral Co(II) site, and an octahedral Co(II) geometry at the other HisB10 site (Brader et al., 1991; Brzovic et al., 1994; Choi et al., 1996).

[3] The observation of a strict 3-fold symmetry holds only for the rhombohedral crystal forms of the insulin hexamer, wherein the asymmetric unit is an insulin dimer. These structures include T_6, T_3R_3, and R_6 species (Smith et al., 1984; Baker et al., 1988; Smith & Dodson, 1992; Ciszak & Smith, 1994; Whittingham et al., 1995). Due to what appears to be crystal packing interactions, the monoclinic forms of the hexamer show slight deviations from exact 3-fold symmetry (Derewenda et al., 1989).

$T_3{}^oR_3{}^o$, and R_6) both in the crystalline state and in solution (Derewenda et al., 1989; Smith & Dodson, 1992a,b; Ciszak & Smith, 1994; Brzovic et al., 1994) and quantitative studies of the T- to R-state transition (Bloom et al., 1995) indicate that, when suitably tailored for the insulin hexamer, the Seydoux, Malhotra, and Bernhard (SMB) model is capable of fully describing the allosteric behavior of the system (Figure 2) (Bloom et al., 1995). The allosteric models of Monod et al. (1965) and Koshland et al. (1966) were found to be incapable of describing the system. Assuming that the phenolic pockets of the R_3 and R_3' trimeric units of R_3R_3' have essentially identical affinities such that the dissociation constants for binding, K_R and K_R', are nearly identical (i.e., $K_R \approx K_R'$)[1] (Bloom et al., 1995), then the SMB model for the insulin hexamer requires three conformational states and four physical constants ($L_o{}^A$, $L_o{}^B$, $K_R{}^o$, and K_R)[1] to describe the ligand-mediated T- to R-state equilibria (Figure 2 and eq 1) (Bloom et al., 1995, 1997). The expression for the fraction of R-state (ρ) is given by the equation:

$$\rho = \frac{0.5L_o{}^B(1+\beta)^3 + (1+\alpha)^6}{L_o{}^B(1+\beta)^3 + (1+\alpha)^6 + (L_o{}^BL_o{}^A)} \qquad (1)$$

where $\alpha = ([P]/K_R)$, $\beta = ([P]/K_R{}^o)$, and [P] is the concentration of the free phenolic ligand. The derivation of this equation is presented in the following paper (Bloom et al., 1997).

Others have undertaken efforts to model the allosteric properties of the insulin hexamer. Jacoby et al. (1993) attempted to model the T_6 to T_3R_3 and T_3R_3 to R_6 transitions by treating these processes as separate MWC-like systems. Birnbaum et al. (1996) developed a series of hierarchical models based on a dimer of trimers representation of the hexamer. In this treatment, Birnbaum et al. assume the negative cooperativity is due to intertrimer interactions and that the phenolic pockets of T_3R_3 are identical to those of R_6, an assumption in contradiction of the available three-dimensional structural information. Both of these groups have failed to take into consideration the heterotropic interactions between the HisB10 anion binding sites and the phenolic pockets either in devising their experiments or in formulating their models.

We present here quantitative studies of dynamic and physical interactions for the binding of 2,6- and 2,7-DHN to both the Co(II)-substituted wild-type and the GluB13−Gln mutant human insulin hexamers under carefully selected conditions including the concentrations and identities of the anion effectors present. The spectroscopic properties of these systems are exploited to further test the validity of the physical constants predicted by the SMB model. We also undertake modeling exercises based on the structures of T_3R_3 and R_6 hexamers to examine possible binding modes for 2,6- and 2,7-DHN. Previous investigation of the T- to R-state transition mediated by phenolic ligands and monovalent anions provided important new insights into the allosteric behavior of the hexamer but did not provide quantitative tests of mechanism (Roy et al., 1989; Brader et al., 1991, 1992; Choi et al., 1993; Brzovic et al., 1994). As an extension of the work of Bloom et al. (1995) and to achieve a more quantitative level of analysis, we use 2,6- and 2,7-DHN as sensitive chromophoric/fluorophoric ligand probes to directly investigate the dynamic process of binding. Bloom et al. (1995) established that the E-B13Q mutation has profound effects on the T_6 to $T_3{}^oR_3{}^o$ and $T_3{}^oR_3{}^o$ to R_6 allosteric transitions. The comparisons of binding to E-B13Q and wild-type insulin presented here demonstrate the sensitivity of ligand binding to changes in the structures of side chains that make up the phenolic binding pockets. It will be shown that the differences in ligand affinity and specificity and the apparent degree of negative cooperative subunit interactions originate from the structural differences in the $T_3{}^oR_3{}^o$ and R_6 binding sites arising from the symmetry properties of these oligomers.

[4] The designation negative cooperativity is used empirically to denote binding isotherms exhibiting shapes consistent with apparent affinities which become weaker as ligand concentration is increased or binding isotherms which appear to saturate at a site occupancy less than the total number of sites (i.e., half-site reactivity).

MATERIALS AND METHODS

Materials. Metal-free E-B13Q recombinant human mutant insulin and wild-type human insulin were supplied by the Novo Research Institute (Bagsvaerd, Denmark). $Co(ClO_4)_2$ (Alfa, Danvers, MA), $CaSO_4$ (Sigma, St. Louis, MO), $ZnSO_4$ (Mallinckrodt, St. Louis, MO), KSCN (Aldrich, Milwaukee, WI), KH_2PO_4 (Fisher), KCl (Sigma), Trizma (Sigma), $HClO_4$ (Mallinckrodt), 2,7-dihydroxynaphthalene (Sigma), 2,6-dihydroxynaphthalene (Aldrich), and phenol (Aldrich) were used without additional purification. Unless otherwise stated, all measurements were performed in 50 mM Tris−perchlorate buffer at pH = 8.00 and 25 °C.

UV−Vis and Fluorescence Studies of 2,6- and 2,7-DHN. Absorbance spectra for 5.0 mM solutions of 2,6- or 2,7-DHN were measured on a HP8452A diode array spectrophotometer equipped with a PC processing system. Two buffer solutions were used: potassium phosphate for pH 2−7 and 10 and Tris−perchlorate for pH 8−9. Emission profiles were determined for 2,6- (λ_{ex} = 326 nm) and 2,7-DHN (λ_{ex} = 310 nm) with a SPEX fluorolog 1680-1681 double monochrometer system and a DMB1 spectroscopy laboratory coordinator.

Rapid-Mixing Stopped-Flow Fluorescence Studies. The fluorescence emission of 2,6-DHN (λ_{ex} = 374 nm) or 2,7-DHN (λ_{ex} = 350 nm) was monitored in both the presence and the absence of 0.2 mM Zn(II)−wild-type insulin hexamers with 50 mM Cl^-. The time courses for the binding of 2,6- and 2,7-DHN were monitored by the change in fluorescence intensity using an Applied Photophysics SFMV17 stopped-flow rapid-mixing unit with customized optical, data acquisition and data analysis systems. Cut-off and cut-on filters were used to isolate the fluorescence emission of the DHN anions (400−550 nm) and to eliminate scattered light and infrared emissions. Time courses were determined for the binding of 2,6- and 2,7-DHN to the Co(II)−insulin hexamer in the presence of 100 mM SCN^-, conditions which give the $T_3{}^oR_3{}^o$ conformation.

UV−Vis Binding Isotherms. Isotherms for the T- to R-state transitions of the Co(II)-substituted wild-type and E-B13Q mutant insulin hexamers driven by the binding of 2,6- and 2,7-DHN were determined as described by Choi et al. (1993) and Bloom et al. (1995). Concentrations of E-B13Q and wild-type insulin were determined by absorbance measurements (ϵ_{280} = 5800 M^{-1} cm^{-1}; Porter, 1953). All of the isotherms were measured in 50 mM Tris−ClO_4 buffer

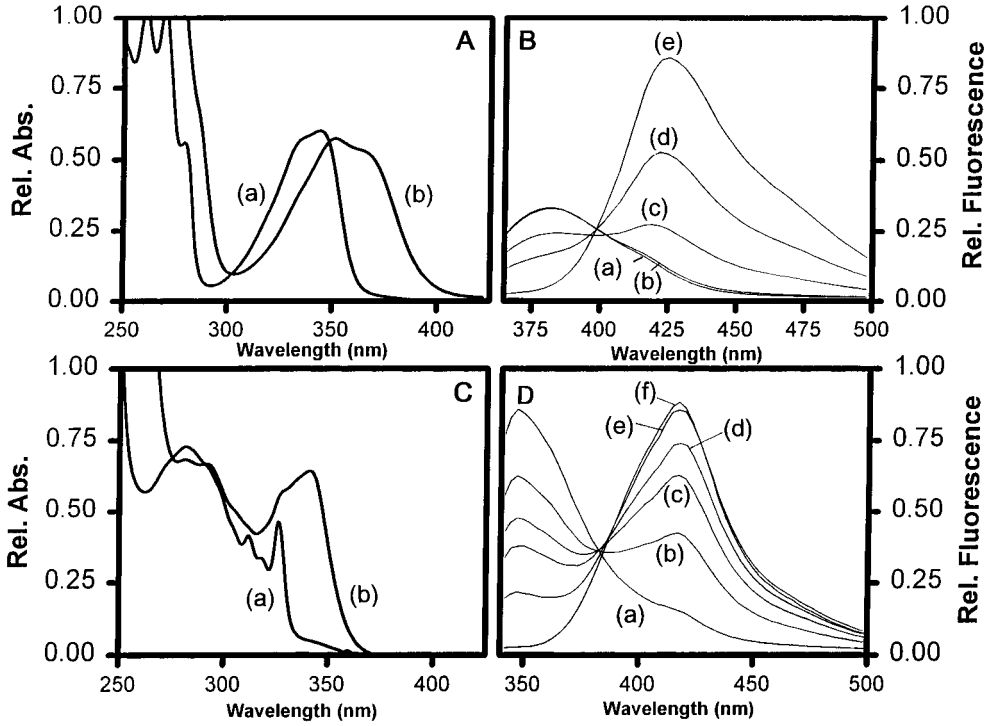

FIGURE 3: UV−vis absorbance spectra and fluorescence emission profiles for 2,6-DHN and 2,7-DHN at 25 °C. Absorbance spectra were recorded for 2.0 mM solutions of (A) 2,6-DHN and (C) 2,7-DHN at (a) pH 8.0 and (b) pH 10.0. Fluorescence emission spectra (B) for 5.0 mM 2,6-DHN at pH (a) 3.0, (b) 4.0, (c) 6.0, (d) 7.0, and (e) 10.0 using an excitation wavelength of 344 nm. Fluorescence emission spectra for 5.0 mM 2,7-DHN (D) at pH (a) 1.0, (b) 2.0, (c) 3.0, (d) 6.0, (e) 7.0, and (f) 10.0 using an excitation wavelength of 326 nm.

solutions at pH. 8.0 using 0.33 mM Co(II)−hexamer concentrations. Titrations of Co(II) wild−type human insulin were performed in the presence of 5 mM $PABA^-$, while E-B13Q titrations were performed with 25 mM Cl^-. The choice of these anions and the concentrations selected were dictated by the strengths of the heterotropic allosteric interactions each anion exerts on the system. Hence, anion concentrations were chosen such that the R-state species formed is either the $PABA^-$ complex or the Cl^- complex. Since the apparent magnitudes of L_o^A and L_o^B are dependent on anion affinity, the values of these parameters can be modulated by anion concentration and structure (Bloom et al., 1995; Choi et al., 1993). Accordingly, anion concentrations were selected such that the total concentration of phenolic ligand at any point in the titration is well approximated by the concentration of the free ligand.[3] The effects of Ca^{2+} on titrations of wild-type Co(II)−hexamer were performed under analogous conditions but with one Ca^{2+} ion per hexamer. Progress curves were measured by monitoring the UV−vis spectral changes in the Co(II) *d*−*d* transitions upon addition of 2,6- and 2,7-DHN as described in Bloom et al. (1995).

Molecular Modeling of Ligand Binding. The ten-carbon, two-ring 2,6-DHN molecule was docked into the phenolic pockets of $T_3{}^oR_3{}^o$ and R_6, using Biosym Industries Insight software on a Silicon Graphics Industries workstation. The three-dimensional structures of the $T_3{}^oR_3{}^o$ and R_6 phenolic binding sites were modeled by applying the Voidoo cavity predicting program (Kleywegt & Jones, 1994) and visualizing with the Silicon Graphics Industries workstation and the program O (Jones et al., 1991). By selectively deleting all residues which do not directly participate in the phenolic binding site and by holding fixed the positions of those residues which contribute to the pocket surface, the $T_3{}^oR_3{}^o$ and R_6 structures have been overlaid. After superimposing 2,6-DHN on the position occupied by the phenol ring, the Discover (Insight II) program was used to predict any H-bonds between 2,6-DHN and the available donors and acceptors in the site.

RESULTS

pH Profiles and Spectroscopic Analysis of 2,6- and 2,7-DHN. UV−vis spectra (Figure 3) were recorded for (A) 2,6- and (C) 2,7-DHN at pH 8.0 and 10.0. Four distinct envelopes are present in each spectrum. 2,6-DHN has envelopes in the 200−250, 250−315, and 315−365 nm ranges at pH 8.0 and a unique envelope arising from the DHN monoanion at 335−385 nm at pH 10.0. 2,7-DHN has envelopes in the 200−250, 250−305, and 305−340 nm ranges at pH 8.0 and a unique envelope at 335−360 nm arising from the monoanion at pH 10.0. Extinction coefficients for 2,6-DHN ($\epsilon_{344} = 2830 \pm 200\ M^{-1}\ cm^{-1}$) and 2,7-DHN ($\epsilon_{326} = 2640 \pm 200\ M^{-1}\ cm^{-1}$) were estimated by comparison to published spectra (UV Index numbers 6410 and 6440; Stadler Research Laboratories, Philadelphia, PA).

In the pH range 2−10, fluorescence emission spectra (Figure 3) of 2,6- (B) and 2,7-DHN (D) each exhibit two emission peaks (380 and 424 nm for 2,6-DHN; 343 and 420 nm for 2,7-DHN). At pH 2.0, the shorter wavelength peaks dominate; at pH 10.0, these are completely converted to the longer wavelength peaks. The 380 nm (2,6-DHN) and 343 nm (2,7-DHN) peaks arise from the neutral forms, while the 424 nm (2,6-DHN) and 420 nm (2,7-DHN) peaks arise from the monoanion forms. The pH profiles of the two peaks allow estimates of the pK_a values for the first ionization; $pK_a{}^1{}_{2,6-DHN} \cong 10.5$ and $pK_a{}^1{}_{2,7-DHN} \cong 9.5$.

Binding of 2,6- and 2,7-DHN to Co(II) Wild-Type and E-B13Q Insulin Hexamers Monitored by UV−Vis Spectroscopy. Isotherms for the binding of 2,6- and 2,7-DHN binding

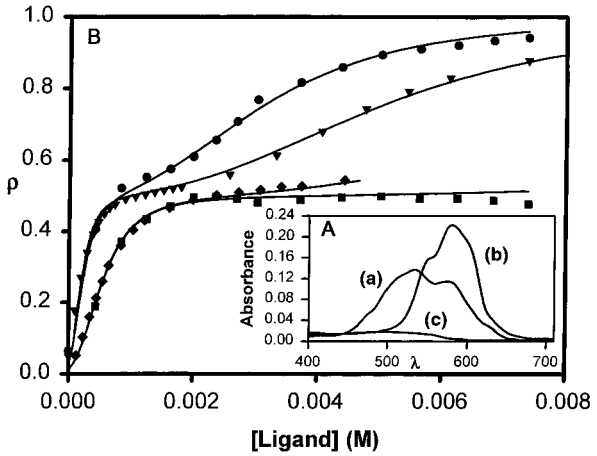

FIGURE 4: (A) UV−vis absorbance spectra of wild-type Co^{2+}-substituted insulin hexamers: the tetrahedral R-state Co(II)−$PABA^-$ complex (a), the tetrahedral R-state Co(II)−Cl^- complex (b), and the octahedral T-state Co(II)−$(H_2O)_3$ complex (c). (B) Ligand titrations for Co(II)-substituted insulin hexamers. Titrations were performed as described by Choi et al. (1993) and Bloom et al. (1995) at 25 °C. The fraction of R-state (ρ) (eq 1) is determined by the relative contributions of R- and T-state Co^{2+} complexes for 0.33 mM hexamer solutions. Plots of ρ vs ligand concentration were determined for (◆) 2,6-DHN or (■) 2,7-DHN binding to the wild-type Co(II) insulin hexamer in the presence of 5 mM $PABA^-$ and for (▼) 2,6-DHN or (●) 2,7-DHN binding to the E-B13Q mutant Co(II) insulin hexamer in the presence of 25 mM Cl^-.

to wild-type and E-B13Q Co(II)-substituted insulin hexamers were determined by measuring the changes in the Co(II) $d-d$ transitions (Brader et al., 1991; Choi et al., 1993; Bloom et al., 1995). Experimental conditions (see Materials and Methods) were chosen such that the free ligand concentration at each point along the curve is approximately equal to the total ligand concentration (i.e., total ligand >> bound ligand). Each titration can be fit by the appropriately scaled spectra of two species, the octahedral T-state species and either the tetrahedral R-state chloride species or the pentacoordinate R-state $PABA^-$ species (Figure 4A). Titration analyses (Bloom et al., 1995) have shown that the absorption changes in the Co(II) spectrum at 572 nm (the Cl^- adduct) or 580 nm (the $PABA^-$ adduct) are proportional to the concentration of R_3 units ($[R_3] \propto \Delta A_{572}$). Titrations of the Co(II) E-B13Q hexamer were performed under analogous conditions but in the presence of 25 mM Cl^-. Computer fitting (Figure 4B, solid lines) using eq 1 gave values for L_o^A, L_o^B, K_R^o, and K_R (Table 1) [see Bloom et al. (1997)] as previously described (Bloom et al., 1995).

Binding of 2,6- or 2,7-DHN to Wild-Type Insulin Hexamers Monitored by Fluorescence. The binding of 2,6- or 2,7-DHN to the insulin hexamer can be directly investigated using changes in the ligand fluorescence emission upon binding (Figure 5A). Excitation of 2,6-DHN at 374 or 344 nm results in emission from the monoanionic form or the neutral form, respectively. Addition of a large excess of Zn(II)−Insulin or Co(II)−Insulin hexamers shifts the emission spectrum completely to the neutral form, indicating that only the neutral species binds to the phenolic pockets (data not shown). The behavior of the system is consistent with that shown in (Scheme 1). In the presence of SCN^-, the Co(II)-substituted wild-type insulin hexamer is converted to a Co(II)−$T_3^oR_3^o$ species with SCN^- coordinated to the tetrahedral R_3−HisB10−Co(II) ion, a hexamer with three water-filled phenolic pockets (Whittingham et al., 1995). SCN^- binding stabilizes the E-B13Q mutant hexamer as a Co(II)−R_6 species with six water-filled pockets (Brzovic et al., 1994). The kinetics of binding (Figure 5B) of both DHNs have been determined by monitoring the loss of fluorescence under pseudo-first-order conditions using an excess of $T_3^oR_3^o$ sites (i.e., [sites]:[DHN] ≥ 10:1). The fluorescence time courses are well described by the rate expression for a single exponential process: $F_t = F_\infty - Fe^{-t/\tau}$, where F is the signal amplitude and F_t and F_∞ are the fluorescence values measured at time t and time ∞, respectively. According to relaxation kinetic theory (Bernasconi, 1976), the simplest mechanism for the linear dependence of $1/\tau$ with respect to the site concentration involves a bimolecular binding process.

Assuming a model for binding to $T_3^oR_3^o$(SCN) where the three phenolic pockets are identical and independent, then over the concentration range accessible to measurement, the dependence of the relaxation rate is linear with respect to the concentration of sites (Figure 5C) and, therefore, is consistent with the equations:

$$\mathrm{DHN} + T_3^oR_3^o(\mathrm{SCN}) \rightleftharpoons T_3^oR_3^o(\mathrm{SCN})(\mathrm{DHN})$$

$$\mathrm{DHN} + T_3^oR_3^o(\mathrm{SCN})(\mathrm{DHN}) \rightleftharpoons T_3^oR_3^o(\mathrm{SCN})(\mathrm{DHN})_2$$

$$\mathrm{DHN} + T_3^oR_3^o(\mathrm{SCN})(\mathrm{DHN})_2 \rightleftharpoons T_3^oR_3^o(\mathrm{SCN})(\mathrm{DHN})_3 \quad (2)$$

Provided $[T_3^oR_3^o(\mathrm{SCN})] >> [\mathrm{DHN}]$, then

$$1/\tau = k_{on}3[T_3^oR_3^o(\mathrm{SCN})] + k_{off} \quad (3)$$

The slope and intercept values obtained from plots of $1/\tau$ versus the concentration of binding sites, three per $T_3^oR_3^o$(SCN) (Figure 5C), give $k_{on} = 6.3 \times 10^5\ M^{-1}\ s^{-1}$ and $k_{off} = 460\ s^{-1}$, respectively, for 2,7-DHN and $k_{on} = 1.65 \times 10^6\ M^{-1}\ s^{-1}$ and $k_{off} = 220\ s^{-1}$, respectively, for 2,6-DHN. Dissociation constants for binding were determined from these rate constants using the expression $K_R^o = k_{off}/k_{on}$ (Table 1).

Effect of Ca^{2+} on the Binding of 2,6- or 2,7-DHN to Wild-Type Co(II)−Insulin Hexamers. Isotherms for binding of 2,6- or 2,7-DHN were measured in the presence and absence of Ca^{2+} (Figure 6A). In the presence of Ca^{2+}, the binding isotherms for the wild-type hexamers shift to lower amplitudes and higher ligand concentrations, and the apparent affinities are weakened approximately 2-fold with no significant change in L_o^A. Analysis of the binding of SCN^- in the presence of Ca^{2+} (Figure 6B) versus SCN^- alone shows a shift to higher amplitudes and lower ligand concentrations, indicating an apparent decrease in the dissociation constant. In the case of competitive binding, the model predicts only a shift to higher ligand concentrations.

Molecular Modeling of 2,6-DHN Binding to $T_3^oR_3^o$ and R_6 Wild-Type Insulin Hexamers. The structures of the phenolic binding sites of the $T_3^oR_3^o$ and R_6 insulin hexamers (Figure 7A) alone and (Figure 7B) with 2,6-DHN bound were modeled using Voidoo, O, and Insight II software (Kleywegt & Jones, 1994; Jones et al., 1991; Biosym Industries). The phenolic pockets of the $T_3^oR_3^o$ (Figure 7A,C in yellow) and R_6 hexamers (Figure 7B,C in white) have nearly identical total volumes of 200 Å^3. The $T_3^oR_3^o$ cavity has an open globular shape that extends from near the hexamer surface down almost to the center of the hexamer. Access to solution

Table 1: Comparison of Allosteric Parameters Obtained from Fitting the T- to R-State Allosteric Transitions of the Wild-Type and E-B13Q Mutant Insulin Hexamers to the Suboptimal Symmetry Model for Negative Cooperativity and Half-Site Reactivity of Seydoux et al. (1974)[a]

	ρ equation values				
phenolic and anionic ligands, insulin species	L_o^A ($\times 10^1$)	L_o^B	K_R^o ($\times 10^{-4}$ M)	K_R ($\times 10^{-4}$ M)	r_2
2,6-DHN					
−WT Co(II) insulin and 5 mM PABA	4 ± 2	$(2 \pm 1) \times 10^7$	2 ± 1	*b*	0.99
−E-B13Q Co(II) insulin and 25 mM Cl^-	2 ± 1	$(5 \pm 2) \times 10^2$	1 ± 0.5	3 ± 1.5	0.99
2,7-DHN					
−WT Co(II) insulin and 5 mM PABA	4 ± 2	$(2 \pm 1) \times 10^7$	2 ± 1	*b*	0.98
−E-B13Q Co(II) insulin and 25 mM Cl^-	2 ± 1	$(5 \pm 2) \times 10^2$	1 ± 0.5	2 ± 1	0.99

	MWC equation values		
	L_o^A ($\times 10^1$)	K_R^o ($\times 10^{-4}$ M)	r_2
2,7-DHN −WT Co(II) insulin and 5 mM PABA	4 ± 2	2 ± 1	0.98
2,6-DHN −WT Co(II) insulin and 5 mM PABA	4 ± 2	2 ± 1	0.99

	kinetic measurement K_R^o ($\times 10^{-4}$ M)
2,7-DHN −WT Co(II) insulin and 100 mM SCN^-	7 ± 3
2,6-DHN −WT Co(II) insulin and 100 mM SCN^-	1 ± 0.5

	preexisting fraction of R-state (%)	
	predicted by ρ values	calculated from spectra
Co(II) wild-type insulin with 5 mM $PABA^-$	1.2 ± 1	4.0 ± 3
Co(II) E-B13Q insulin with 25mM Cl^-	2.5 ± 2	5.5 ± 4

[a] The data are derived from equilibrium and kinetic studies for the binding of the allosteric effectors 2,6- and 2,7-DHN to the R-state PABA and chloride ion complexes at pH 8.0 and 25 °C. The allosteric forms of the insulin hexamer are designated T_6, T_3R_3, and R_6 in accord with the nomenclature developed by Kaarsholm et al. (1989). The nomenclature of Monod et al. (1965), Kaarsholm et al. (1989), and Brzovic et al. (1995) is used here to designate the two different subunit conformations of the R_6 hexamer. [b] The microscopic dissociation constant for the R_3 and R_3' state (K_R) could not be determined from the wild-type insulin titrations due to the lack of a specific signal for each binding process.

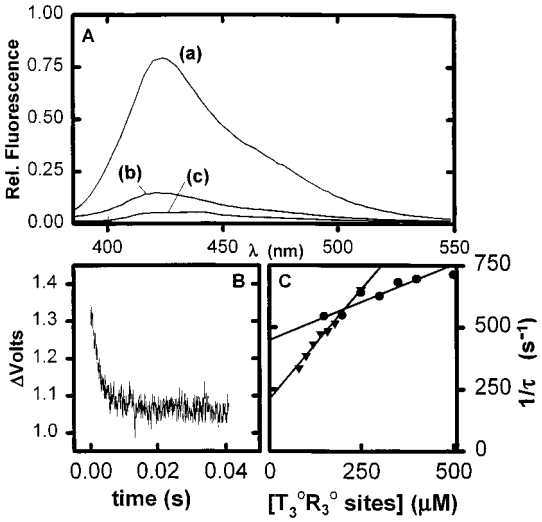

FIGURE 5: Changes in fluorescence of 2,6-DHN. (A) Fluorescence emission profile (λ_{ex} = 374 nm) of (a) 0.1 mM 2,6-DHN alone, (b) 0.1 mM 2,6 DHN in the presence of 0.167 mM Zn(II) insulin hexamers with 5 mM $PABA^-$, and (c) 5 mM $PABA^-$ alone. (B) Stopped-flow fluorescence decay time course (λ_{ex} = 374 nm) for the reaction of 10 μM 2,6-DHN with 100 μM wild-type $T_3^oR_3^o$ insulin hexamer sites (see Discussion). (C) Dependence of the rate of fluorescence emission decay on the site concentration for the reaction of (▼) 2,6-DHN and (●) 2,7-DHN following mixing with wild-type Co(II) insulin hexamers under $T_3^oR_3^o$ conditions at 25 °C (see discussion).

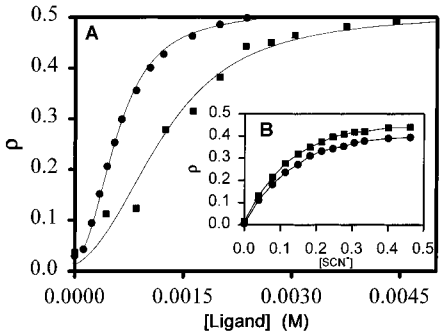

FIGURE 6: Ligand titrations at 25 °C for Co(II)-substituted wild-type insulin hexamers for (A) 2,6-DHN in the (●) absence and (■) presence of Ca^{2+} (one per hexamer) and (B) SCN^- in the (●) absence and (■) presence of Ca^{2+} (one per hexamer).

Scheme 1

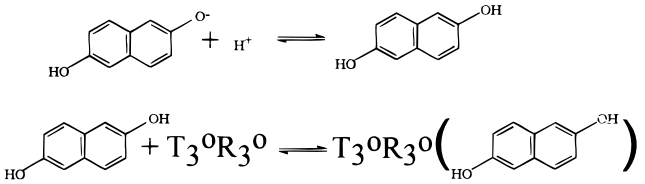

is via a narrow opening with dimensions somewhat smaller than the van der Waals cross section of phenol. The R_6 cavity has a less open shape that is restricted in the center which also extends from near the hexamer surface down almost to the center of the hexamer. For both structures, residues CysA6 and CysA11 from molecule I are shown which provide H-bonds to phenol at one end of the cavity along the dimer−dimer interface. In the R_6 structure, the cavity extends ~8 Å beyond phenol to GluB13 from molecule II of the adjacent dimer to the core of the hexamer (Figure 7, lower right, in white). The residues surrounding phenol include CysB7, HisB10, LeuB11, AlaB14, IleA10, and GluB13 from molecule I and ValB2, HisB5, and LeuB17 from the adjacent molecule I, as well as GluB13 from molecule II. In the R_6 crystal structure, the unfilled portion of the cavity between the phenol ring and the GluB13 carboxylates is occupied by two water molecules (Smith & Dodson, 1992a,b). Modeling studies with the $T_3^oR_3^o$ structure revealed that there are several allowable orientations of 2,6-DHN in the pocket. On the basis of surface contacts

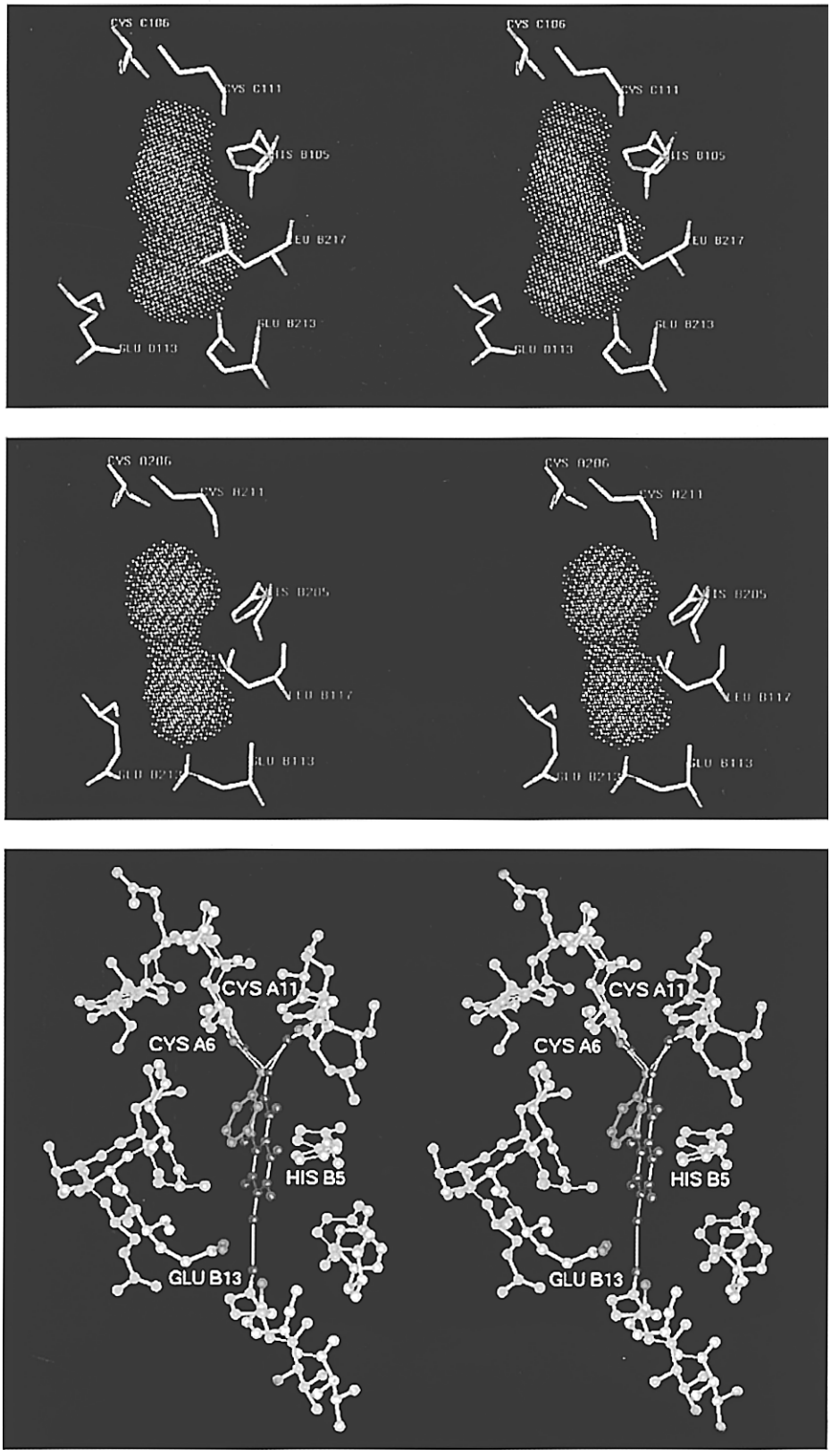

FIGURE 7: Stereo diagrams of the (A, top) calculated accessible volume of a $T_3{}^oR_3{}^o$ phenolic binding site, (B, middle) calculated accessible volume of a R_3R_3' phenolic binding site, and (C, bottom) differences between the phenolic binding sites of $T_3{}^oR_3{}^o$ (yellow) and R_3R_3' (white) of the wild-type insulin hexamer with the crystallographically determined position of phenol (green) and the hypothesized binding position of 2,6-DHN (red) predicted by modeling. H-bonds are shown to CysA11, CysA6, and GluB13.

and H-bonding, Figure 7C shows the most favorable orientation. In this model, three software-predicted H-bonds involving the hydroxyls of DHN and CysA11, CysA6, and GluB13 of molecule I of the $T_3{}^oR_3{}^o$ conformation are shown (H-bonds not shown to the R_6 conformation). The GluB13 side chain from molecule II is located >2 Å deeper in the pocket and does not appear to be within H-bonding distance of the DHN hydroxyl group. This model shows that it is plausible that the two hydroxyl groups and the naphthalene ring of 2,6-DHN fill most of the pocket, that favorable van

der Waals contacts exist with the hydrophobic side chains lining the pocket, and that the ring surface makes contact with HisB5.

In Figure 7C, the structure of the $T_3{}^oR_3{}^o$ binding site (in yellow) has been overlaid on the R_6 site to show the structural differences. As with R_6, the binding site is primarily formed by residues at the dimer−dimer interface from two adjacent molecule I R-state monomers. Small changes in the positions of side chains from molecule I occur near CysA6 and CysA11 (<1.0 Å), but these do not significantly change the structure of the site or the potential for these residues to form H-bonds with the 2-hydroxyl of 2,6-DHN. The most significant changes occur deep in the pocket. Changes in residues LeuB11 and GluB13 from molecule I (Figure 7, left side) and GluB13 from T-state molecule II give a site in which the most favorable H-bond is between the 6-hydroxyl of 2,6-DHN and a T-state GluB13 carboxylate (O−H−O bond length of 2.7 Å; Figure 7). The distance to the GluB13 side chain of molecule I is changed to 6.3 Å, making H-bonding to this residue unlikely. Changes at the dimer−dimer interface make the pocket significantly less constricted.

DISCUSSION

Model Testing of the Allosteric Properties of the Insulin Hexamer. The insulin hexamer has proven to be a valuable model system for the investigation of the allosteric properties of oligomeric protein complexes. The hexamer possesses nearly every classic mode of cooperativity, including positive and negative homotropic[4]and heterotropic interactions and half-site reactivity (Brader et al., 1991; Choi et al., 1993; Brzovic et al., 1994; Bloom et al., 1995). Quantitation of ligand binding to the phenolic pockets has provided the means for testing the mechanism of the allosteric transition. Evidence in the form of structural, binding, ^{1}H-NMR, and spectroscopic data is consistent with the SMB model; while the model, of Koshland et al. (1966) is inconsistent with these data. The observation of negative cooperativity disqualifies the MWC model.

The SMB and KNF models differ in several key interpretations of allosteric phenomena. The KNF model is based on the fundamental assumption that all ligated conformations are induced by reciprocal interactions between the protein and the specific ligands to create the ligand site. As originally formulated, the model does not allow for the existence of a protein conformation with specific, preformed ligand binding sites; i.e., the KNF model postulates that ligand binding induces the new subunit conformation. In contrast, the SMB model postulates a preexisting equilibrium between different conformational states that can be shifted by mass action due to preferential ligand binding to one of the states. In the case of the insulin hexamer, the equilibrium between the extremely low affinity state (T) and the high-affinity state (R) has been shown to exist in the absence of phenolic ligands (Brader et al., 1991; Brzovic et al., 1994; Bloom et al., 1995; Choi et al., 1996).

The most persuasive evidence in support of an SMB model for the insulin hexamer resides in the symmetry properties within the trimeric units of the rhombohedral crystalline forms of the hexamer.[3] Each dimeric unit possesses small variations in positions of side chain residues, giving a pseudo-2-fold symmetry axis. This variation from exact 2-fold symmetry is designated as T_3T_3' or R_3R_3' (Kaarsholm et al., 1989). However, as postulated by the SMB model, these small differences are maintained about the true 3-fold symmetry axis.[3] The 3-fold symmetry axis is conserved in all rhombohedral X-ray crystal structures of the hexamer,[3] including the unligated, fully ligated, and various mutant hexamers (Smith et al., 1984; Baker et al., 1988; Derewenda et al., 1989; Smith & Dodson, 1992a,b; Whittingham et al., 1995). Consequently, it is appropriate to assign the insulin hexamer a concerted, symmetry-conserved, three-conformation-state equilibrium.

Bloom et al. (1995) have shown that, for the insulin system, the SMB model for allostery quantitatively describes the mixed positive and negative homotropic cooperative effects of phenolic compounds and can accommodate the heterotropic effects of anion binding. In order to independently verify the equilibrium values predicted by the model, in this investigation we present independent measurements of the dissociation constants. To accomplish these studies, the optical properties of 2,6- and 2,7-DHN have been exploited to provide quantitative signals that directly measure the binding of these ligands to the phenolic pockets of the insulin hexamer. To complement these experiments, we also present spectroscopic evidence and molecular modeling to predict the three-dimensional structure of the 2,6-DHN−insulin hexamer complex.

Fraction of R-State Equation. The equation for the fraction of R-state species (ρ) predicted by the SMB model (eq 1) is matched to the specific properties of the insulin hexamer (Bloom et al., 1995,1997). Our preliminary studies established that $K_R \approx K_R'$, and that eq 1 is capable of quantifying the relationship between the more than one hundred possible species of ligand-bound hexamer and the concentration of free phenolic ligand. *This large number of statistically possible ligation states is described using four variables, $L_o{}^A$, $L_o{}^B$, $K_R{}^o$, and K_R, which, according to the SMB model, are true microscopic physical constants.* $L_o{}^A$ and $L_o{}^B$ are the allosteric equilibrium constants for the conversion of T_6 to $T_3{}^oR_3{}^o$ and for the conversion of $T_3{}^oR_3{}^o$ to R_6, respectively; $K_R{}^o$ and K_R are the specific dissociation constants for the binding of phenolic ligands to the $T_3{}^oR_3{}^o$ and R_6 phenolic sites, respectively (Figure 2) [see Bloom et al. (1997)].

Since eq 1 is based on the fraction of subunits in the R-state, the spectroscopic properties of the Co(II)−insulin hexamer system are well suited for collecting experimental data. With the exception of a Zn(II)−T_3R_3 hexamer grown in the presence of 0.75 M chloride ion (Ciszak & Smith, 1994),[2] the ligand field geometry is dictated by the protein conformation (Derewneda et al., 1989; Smith & Dodson, 1992; Roy et al., 1989; Brader et al., 1991, 1996; Brzovic et al., 1994; Bloom et al., 1995). Consequently, the changes in the Co(II) $d-d$ transitions associated with the conversion from octahedral (T-state) to tetrahedral (R-state) are directly correlated to the concentration of R_3 units (Choi et al., 1993, 1996; Bloom et al., 1995). This signal has been used to determine isotherms for the binding of 2,6-DHN (Bloom et al., 1995) and 2,7-DHN (Figures 4 and 5) to wild-type and E-B13Q insulin hexamers.

Analysis of the Binding Isotherms. The binding isotherms presented in Figures 4B and 6A are illustrative of the full range of allosteric properties exhibited by the insulin hexamer. From casual inspection of the curves for wild-type insulin in Figures 4A and 6A, it is obvious that the

initial phase (0 to ~1.0 mM DHN) of each of the curves is sigmoidal, implying a positive cooperative behavior. At higher ligand concentrations (>2 mM DHN) (Figure 4A), the 2,7-DHN curve appears to plateau at $\rho \approx 0.5$, while the 2,6-DHN curve tends to plateau at $\rho \approx 0.5$, but then at higher concentrations rises slightly above $\rho = 0.5$. Both curves imply a half-site reactivity/negative cooperative behavior. In marked contrast to the behavior of wild-type insulin, the curves for the E-B13Q mutant hexamer (Figure 4A) show an initial phase that is slightly sigmoidal, a tendency to plateau at $\rho \approx 0.5$, followed by a second sigmoidal phase which approaches $\rho \approx 1.0$ at high DHN concentration. Computer fitting of the isotherms in Figures 4 and 6 to eq 1 gives values of the four microscopic equilibrium variables, L_o^A, L_o^B, K_R^o, and K_R (Table 1). These analyses provide the basis for several important conclusions: (a) The seemingly complex shapes of the isotherms for the E-B13Q mutant hexamer can be adequately described by a four-parameter model. (b) Because the second phase is missing or insignificant, K_R could not be determined for the wild-type hexamer, and the isotherms for 2,6- and 2,7-DHN are adequately described by three parameters (L_o^A, L_o^B, and K_R^o), whereas the isotherms for the E-B13Q mutant require four parameters. (c) The values of L_o^A and L_o^B obtained from fitting the DHN isotherms for both wild-type and E-B13Q mutant insulins are in good agreement with values previously reported for phenol, resorcinol, and cyclohexanol, ligands which give quite different isotherms (Bloom et al., 1995). (d) Because the $T_3^oR_3^o$ to R_3R_3' allosteric transition is made more favorable by a factor of 4×10^4 by the E-B13Q mutation, the isotherms for 2,6- and 2,7-DHN approach full-site reactivity. (e) The SMB model provides a very satisfactory description of these isotherms. While the behavior of the DHN isotherms with the wild-type insulin hexamer could be explained by the simple three-state MWC model, these data show that a simple mutation of Glu to Gln at B13 reveals a more complex behavior that cannot be explained by the MWC model. When the DHN isotherms of wild-type and E-B13Q mutant hexamers are considered together, it is clear that the apparent half-site reactivity of the wild-type system arises from a combination of an energetically unfavorable $T_3^oR_3^o$ to R_3R_3' allosteric transition ($L_o^B = 2 \times 10^7$) and reduced affinities for R_3R_3' in comparison to $T_3^oR_3^o$.

Verification of L_o^A and L_o^B. The conformational equilibrium constants, L_o^A and L_o^B determined by Bloom et al. (1995), are independently verified by spectral analysis (Figure 4A, Table 1). Comparison of the amounts of T- and R-state species preexisting in the absence of phenolic ligands gives an overall measure of the equilibrium which can be related to L_o^A and L_o^B by the equation:

$$[\text{R-state}]/[\text{T-state}] = \frac{0.5(1/L_o^A) + (1/L_o^A L_o^B)}{0.5(1/L_o^A) + 1} \quad (4)$$

For example, in the case of the wild-type hexamer, when the Co(II) ligand is PABA, L_o^A is 40 and L_o^B is 2×10^7; consequently, the equation simplifies to [R-state]/[T-state] $= 0.5(1/L_o^A)$. All titrations measured in the presence of 5 mM PABA gave values in agreement with this relationship.

Measurement of K_R^o for 2,6- and 2,7-DHN. Verification of the dissociation constants determined by computer analysis of binding isotherms (Figure 4B, Table 1, eq 1) for the binding of phenolic compounds presents a more difficult task. Since most phenolic compounds stabilize the formation of both the $T_3^oR_3^o$ and R_6 hexamers, there is no easy way to distinguish binding to these two states. However, the binding of 2,6- or 2,7-DHN to the wild-type hexamer gives the $T_3^oR_3^o$ conformation almost exclusively. In the absence of other ligands, high SCN^- concentrations also stabilize the $T_3^oR_3^o$ conformation, giving an R_3^o unit with a pseudotetrahedral $Co(II)(His)_3SCN^-$ adduct at the R_3 metal site and three unoccupied phenolic pockets (Whittingham et al., 1995). If the SMB model for insulin (Figure 2) is correct, then the preformed phenolic pockets of the R_3^o unit should behave as identical and independent binding sites with an affinity for DHN described by the equation:

$$T_3^oR_3^o(SCN^-) + DHN \underset{k_{-1}}{\overset{k_1}{\rightleftharpoons}} T_3^oR_3^o(SCN^-)(DHN) \quad (5)$$

where the statistically corrected expressions for the microscopic dissociation constant are given by the equation:

$$K_R^o = 3[T_3^oR_3^o(SCN^-)][DHN]/[T_3^oR_3^o(SCN^-)(DHN)] = [T_3^oR_3^o(SCN^-)(DHN)][DHN]/[T_3^oR_3^o(SCN^-)(DHN)_2] = [T_3^oR_3^o(SCN^-)(DHN)_2][DHN]/3[T_3^oR_3^o(SCN^-)(DHN)_3] = k_{-1}/k_1 \quad (6)$$

The fluorescence changes that accompany binding of 2,6- and 2,7-DHN were examined both by single-wavelength stopped-flow kinetics and by equilibrium binding. When excited at pH 8.0, the fluorescence emission profiles (Figure 5) of 2,6- (A) and 2,7-DHN (B) show peaks arising from excitation of the neutral forms ($\lambda_{em}^{2,6-DHN} = 380$ nm; $\lambda_{em}^{2,7-DHN} = 343$ nm) and the monoanionic forms ($\lambda_{em}^{2,6-DHN} = 424$ nm; $\lambda_{em}^{2,7-DHN} = 424$ nm). By using excitation wavelengths specific for the anions, emission from the anionic species occurs without contributions from the neutral species. Since only the neutral (protonated) forms of 2,6- and 2,7-DHN bind to the phenolic pockets, the intensities of the DHN emissions measure the concentrations of the free anions and thus serve as indicators of binding.

When monitored using a stopped-flow fluorometer, the observed time courses for the binding of 2,6- and 2,7-DHN occur as single exponential decay processes ($1/\tau_1$) (eqs 2 and 3; Figure 5C). If this mechanism is correct, then k_{on} and k_{off} for the binding process are given by the slope and intercept, respectively. These values are as follows: $k_{on} = 6.3 \times 10^5\ M^{-1}\ s^{-1}$ for 2,6-DHN and $1.65 \times 10^6\ M^{-1}\ s^{-1}$ for 2,7-DHN; $k_{off} = 460\ s^{-1}$ for 2,6-DHN and $220\ s^{-1}$ for 2,7-DHN (Figure 6C). The kinetically determined dissociation constants calculated as $K_D = k_{off}/k_{on} = k_{-1}/k_1$ (eq 6, Table 1) provide a direct measure of K_R^o for the binding of each DHN. The K_R^o values obtained by computer fitting to the proposed allosteric model (eq 1) are similar to those obtained from the determination of k_{on} and k_{off}.

The E-B13Q Mutation Strongly Alters L_o^B. The ^{1}H-NMR studies of Roy et al. (1989) provided qualitative evidence that mutation of GluB13 to Gln strongly affected the allosteric properties and stability of the insulin hexamer. In

solution, both metal ion-free and Zn(II)-substituted E-B13Q systems give predominantly the T_6 state, while phenol stabilizes the R_6 species. The crystalline Zn(II) complex forms a T_6 hexamer, but in the absence of Zn(II), the T_3R_3 state crystallizes (Bentley et al., 1992). Bloom et al. (1995) were able to quantify the effects of this mutation on L_o^A, L_o^B, K_R^o, and K_R. The work presented in Figure 4 and Table 1 extends these observations to the 2,6- and 2,7-DHN systems in the presence of PABA under conditions where the parameters can be directly compared for both wild-type and mutant hexamers. Comparison of the data given in Table 1 shows that the E-B13Q mutation causes a 4×10^4-fold effect on L_o^B, while the effect on L_o^A is small (the T_3T_3' to $T_3^oR_3^o$ transition is made more favorable by ~2X), and the effects on K_R^o and K_R are negligible. It is well-known that mutations in an allosteric protein can bring about large changes in the cooperativity properties of the oligomer [viz. Perutz (1989); Eisenstein et al. (1990)]. The magnitude of the effect of the E-B13Q mutation on L_o^B implies that the alleviation of unfavorable charge−charge interactions among the GluB13 carboxylates is the dominant effect (Bloom et al., 1995). Conversion of Glu to Gln could also introduce new H-bonding interactions which make significant contributions to the enhanced stability of the hexamer and the R_3R_3' state (Rahuel-Clermont et al., 1997). The finding that the effect on L_o^B depends on the concentration of the anionic ligand, decreasing from 7 orders of magnitude (Bloom et al., 1995) to a little more than 4 orders of magnitude (Table 1) as the PABA concentration is increased from 5 to 25 mM demonstrates that binding interactions at the HisB10 metal ion site strongly influence the energetics of the T_3T_3' to $T_3^oR_3^o$ transition.

Molecular Modeling of DHN Binding. Using the available biochemical and structural data, molecular modeling of 2,6-DHN binding to the insulin hexamer was performed. The X-ray structure of the R_6−phenol complex provided the primary template for positioning 2,6- and 2,7-DHN. Previous ^{1}H-NMR investigations of the phenol−insulin complex show that the anisotropic ring current effects of the phenol ring cause an upfield shift of the HisB5 C4 imidazole ring proton resonance (Brzovic et al., 1994). The same pattern is observed in the DHN complexes, establishing that the location of a DHN ring must be very similar to the location of phenol (Bloom et al., 1995). In agreement with these data, the naphthalene rings can be positioned in the hydrophobic pocket to give favorable van der Waals contacts with the ring C4 of HisB5 and other residues (Figure 7C). This location places the HisB5 C4 proton over the naphthalene ring with an orientation predicted to cause the resonance of this proton to be shifted upfield. The combination of increased surface contacts and additional H-bonding capacity is consistent with the increased affinity of the DHNs compared to phenol. In this model, one hydroxyl group is located within H-bonding distance of the carbonyl oxygen of CysA6 and the amide N−H of CysA11 in the same manner as found in the phenol complex, while the other hydroxyl group could be positioned within H-bonding distance of the GluB13 carboxylate by adjusting the tilt of the naphthalene ring system (Figure 7C).

Effect of Ca^{2+} on the Properties of Wild-Type Insulin Hexamers. ^{113}Cd-NMR spectroscopy (Sudmeier et al., 1981), solution UV/vis spectroscopy (Storm & Dunn, 1985), and X-ray crystallography (Hill et al., 1991) have established that divalent metal ions such as Cd^{2+}, Pb^{2+}, and Ca^{2+} bind to the GluB13 carboxylates of the T_6 hexamer. Choi et al. (1993) have shown that the equilibration among T_6, $T_3^oR_3^o$, and R_6 species for the wild-type insulin hexamer is shifted in favor of the $T_3^oR_3^o$ and R_6 states by Ca^{2+} binding. Since the GluB13 side chains are unlikely to accommodate both H-bonding to DHN and coordination to Ca^{2+} at the same time, binding of Ca^{2+} would interfere with the H-bonding to 2,6- or 2,7-DHN. The binding studies performed in the presence and absence of Ca^{2+} (Figure 6) establish that the affinity for 2,6- and 2,7-DHN decreases in the presence of Ca^{2+}. Molecular modeling of the DHN complexes (Figure 7) predicts an H-bond between the GluB13 carboxylate with one hydroxyl from 2,6- or 2,7-DHN. The proposed H-bonding is consistent with the reduction in the affinities of 2,6- and 2,7-DHN brought about by Ca^{2+} and strongly suggests these ligands compete with Ca^{2+} for the same GluB13 carboxylate residue. The increase in affinity found for other phenolic ligands in the presence of Ca^{2+} is consistent with this prediction since these ligands are unable to H-bond to the GluB13 carboxylate.

Structural Origins of Negative Cooperativity and Half-Site Reactivity in the Insulin Hexamer. The SMB model for insulin predicts that the phenolic pockets of $T_3^oR_3^o$ and R_6 should exhibit different affinities for a given ligand. Although the pseudo-2-fold symmetry of R_6 gives two classes of phenolic sites within the R_6 hexamer, these structural differences are minor and the two R_6 sites are nearly identical. As a result of the structural differences in the T−R and R−R dimer−dimer interfaces which form the $T_3^oR_3^o$ and R_6 binding sites, the $T_3^oR_3^o$ site is significantly less constricted compared to the R_6 sites. Comparison of the X-ray structures of $T_3^oR_3^o$ and R_6 shows that in R_6 (*vida infra*) a shift in the side chains of LeuB11 and GluB13 restricts the size of the cavity such that the phenolic pockets of $T_3^oR_3^o$ are significantly larger than those of R_6 (viz. Figure 7). We propose that 2,6- and 2,7-DHN bind preferentially to this larger site structure and thereby stabilize the $T_3^oR_3^o$ state. The parameters K_R^o, L_o^A, and L_o^B obtained from fitting the isotherms to eq 1 (Table 1) have been verified by independent kinetic and equilibrium measurements. Therefore, this work confirms that the fraction of R-state (ρ) equation provides an appropriate description of the binding of phenolic compounds to the insulin hexamer. The insulin hexamer represents a significant model system that adheres to the principles of pairwise structural asymmetry and symmetrical oligomerization of asymmetric dimers developed by Seydoux et al. (1974). The rules of the SMB model provide more than just a means of describing the allosteric transitions. By quantitatively modeling the mechanism using four variables with defined chemical meanings and by using a rational structure-based approach, it has been possible to correlate both the effects of mutations in the structure of the monomer and structural variations in the phenolic ligands with the resulting alternations in allosteric behavior. We suggest that the SMB model may prove to be of more general significance for describing the allosteric properties of enzymes such as phosphofructokinase (Deville-Bonne & Garel, 1992; Shirakihara & Evans, 1988) and aspartate transcarbamylase (Eisenstein et al., 1990) where there is evidence of concerted allosteric transitions and negative[2] cooperative behavior or half-site reactivity that exclude an MWC model.

In a recent study of the stability of various insulin hexamer species using isothermal titration calorimetry, Birnbaum et al. (1996) modeled the effects of phenol, *m*-cresol, and resorcinol on thermal denaturation of the insulin hexamer. These studies clearly show a significant effect on the second allosteric transition by the first. In our studies (Bloom et al., 1995, and the work presented herein), the finding of a difference in the equilibrium constants of 1×10^7 for the two allosteric transitions of the wild-type hexamer demonstrates how strong this effect can be. Birnbaum et al. attribute the negative homotropic allosteric effect to intertrimer negative cooperativity that is independent of the nature of the phenolic ligands. Our model predicts that the negative cooperativity effects arise from stabilization of the T_3R_3 conformation resulting from a higher phenolic ligand affinity for T_3R_3 binding sites compared to $R_3R'_3$ sites. According to the SMB model for half-site reactivity, the occurrence of oligomer conformations with half of the sites preexisting in a high-affinity form is the result of structural asymmetry. *The nature of unfavorable interactions between the two trimeric units is therefore a function of both the protein structure and the affinity of the phenolic ligands.* Thus, it follows that the choice of ligands is an important factor in determining the most appropriate model for the insulin hexamer. The model proposed by Birnbaum et al. assumes that the affinities for all R-state binding sites are the same for any given phenolic ligand. However, our analysis of the structures of the T_3R_3 and R_6 phenolic binding sites clearly shows that the sites are different, a finding consistent with the pronounced dependence of the isotherm shape on ligand structure (viz. Figure 4). Since the most prominent structural differences in the T_3R_3 and R_6 binding sites reside near the middle of the pocket (viz. Figure 7), smaller ligands, such as phenol, *m*-cresol, or resorcinol, which are confined to one lobe of the cavity where the structural differences are minimal between the T_3R_3 and R_6 states are not diagnostic of this difference. As a result, their microscopic affinities for T_3R_3 vs R_6 change by less than a factor of 2 (see Table 1), whereas larger ligands (i.e., 2,6- and 2,7-DHN) show larger differences in affinities and, therefore, are appropriate probes for discriminating between allosteric models.

The assignment of an allosteric mechanism for the insulin hexamer has implications regarding its biological role. It is likely that the interplay between the three-conformational-state equilibrium and the crystallization of hexamers in storage vesicles is important for stabilizing the hexamer *in vivo*. The allosteric properties of the hexamer may assist the deposition of large, chemically and thermodynamically stable quantities of insulin in small-volume vesicles that are quickly released in response to elevated blood glucose levels. Although definitive biochemical evidence concerning the *in vivo* function of insulin allosterism is lacking, the results obtained from quantitation of the negative cooperative behavior and half-site reactivity suggest that symmetry and pairwise pseudosymmetry are biologically important properties of insulin.

Previous treatments of nearly all systems possessing any deviation from true MWC-type behavior have been carried out with the presumption that a KNF model is the model of choice. In view of the results presented herein and in Bloom et al. (1995, 1997), it is clear that a reexamination of many allosteric systems according to the SMB model may prove to be beneficial to understanding the role of symmetry and asymmetry in the control of biological systems.

ACKNOWLEDGMENTS

We thank Dr. G. David Smith for providing some of the hexamer coordinates used in the production of figures and for modeling binding interactions at the phenolic pockets. We thank Dr. Robert Scavetta for assistance with the cavity volume determinations. We also thank Dr. Wonjae E. Choi for help in preparing Figure 1.

REFERENCES

Baker, E. N., Blundell, T. L., Cutfield, J. F., Cutfield, S. M., Dodson, E. J., Dodson, G. G., Hodgkin, D. C., Hubbard, R. E., Isaacs, N. W., Reynolds, C. D., Sakabe, K., Sakabe, N., & Vijayan, N. M. (1988) *Philos. Trans. R. Soc. London B 319*, 369−456.

Bentley, G. A., Brange, J., Derewenda, Z., Dodson, E. J., Dodson, G. G., Markussen, J., Wilkinson, A. J., Wollmer, A., & Xaio, B. (1992) *J. Mol. Biol. 228*, 1163−1176.

Bernasconi, C. F. (1976) *Relaxation Kinetics*, Academic Press Inc., London.

Birnbaum, D. T., Dodd, S. W., Saxberg, B. E. H., Varshavsky, A. D., & Beals, J. M. (1996) *Biochemistry 35*, 5366−5378.

Bloom, C. R., Choi, W. E., Brzovic, P. S., Ha, J. J., Huang, S-T, Kaarsholm, N. C., & Dunn, M. F. (1995) *J. Mol. Biol. 245*, 324−330.

Bloom, C. R., Kaarsholm, N. C., Ha, J., & Dunn, M. F. (1997) *Biochemistry 36*, 12759−12765.

Blundell, T., Dodson, G., Hodgkin, D., & Mercola, D. (1972) *Adv. Protein Chem. 26*, 279−402.

Brader, M. L., Kaarsholm, N. C., Lee, R. W.-K., & Dunn, M. F. (1991) *Biochemistry 30*, 6636−6645.

Brader, M. L., Borchardt, D., & Dunn, M. F. (1992) *J. Am. Chem. Soc. 114*, 4480−4486.

Brader, M. L., Kaarsholm, N. C., Harnung, S. E., & Dunn, M. F. (1997) *J. Biol. Chem. 272*, 1088−1094.

Brzovic, P. S., Choi, W. E., Borchardt, D., Kaarsholm, N. C., & Dunn, M. F. (1994) *Biochemistry 33*, 13057−13069.

Choi, W. E. (1994) Doctoral Dissertation, University of California, Riverside, Riverside, CA.

Choi, W. E., Brader, M. L., Aguilar, V., Kaarsholm, N. C., & Dunn, M. F. (1993) *Biochemistry 32*, 11638−11645.

Choi, W. E., Borchardt, D., Kaarsholm, N. C., Brzovic, P. S., and Dunn, M. F. (1996) *Proteins: Struct., Funct., Genet. 26*, 377−390.

Ciszak, E., & Smith, G. D. (1994) *Biochemistry 33*, 1512−1517.

Derewenda, U., Derewenda, Z., Dodson, E. J., Dodson, G. G., Reynolds, C. D., Smith, G. D., Sparks, C., & Swensen, D. (1989) *Nature 338*, 594−596.

Deville-Bonne, D., & Garel, J.-R. (1992) *Biochemistry 31*, 1695−1700.

Dodson, E. J., Dodson, G. G., Hubbard, R. E., Moody, P. C. E., Turkengurg, J., Whittingham, J., Xiao, B., Brange, J., Kaarsholm, N., & Thøgersen, H. (1993) *Philos. Trans. R. Soc. London, A 345*, 153−164.

Eisenstein, E., Markby, D. W., & Schachman, H. K. (1990) *Biochemistry 29*, 3724−3731.

Hill, C. P., Dauter, Z., Dodson, E. J., Dodson, G. G., & Dunn, M. F. (1991) *Biochemistry 30*, 917−924.

Jacoby, E., Kruger, P., Karatas, J., & Wollmer, A. (1993) *Biol. Chem. Hoppe-Seyler 374*, 877−885.

Jones, T. K., Zou, J. Y., Cowan, S. W., & Kjeldgaard, M. (1991) *Acta Crystallogr. A47*, 110−119.

Kaarsholm, N. C., Ko, H.-C., & Dunn, M. F. (1989) *Biochemistry 28*, 4427−4435.

Kaarsholm, N. C., Havelund, S., & Hougaard, P. (1990) *Arch. Biochem. Biophys. 283*, 496−502.

Kleywegt, G. J., & Jones, T. K. (1994) *Acta Crystallogr. D50*, 178−185.

Koshland, D. E., Nemethy, G., & Filmer, D. (1966) *Biochemistry 5*, 365−385.

Ludvigsen, S., Roy, M., Thøgersen, H., & Kaarsholm, N. C. (1994) *Biochemistry 33*, 7998−8006.
Monod, J., Wyman, J., & Changeux, J.-P. (1965) *J. Mol. Biol. 12*, 88−118.
Perutz, M. F. (1989) *Q. Rev. Biophys. 22*, 139−237.
Porter, R. R. (1953) *Biochem. J. 53*, 320−328.
Rahuel-Clermont, S., French, C. A., Chou, C. I., Kaarsholm, N. C., & Dunn, M. F. (1997) *Biochemistry 36*, 5837−5845.
Roy, M., Brader, M. L., Lee, R. W.-K., Kaarsholm, N. C., Hansen, J., & Dunn, M. F. (1989) *J. Biol. Chem. 264*, 19081−19085.
Seydoux, F., Malhotra, O. P., & Bernhard, S. A. (1974) *CRC Crit. Rev. Biochem. 2*, 227−257.
Shirakihara, Y., & Evans, P. R. (1988) *J. Mol. Biol. 204*, 973−994.
Smith, G. D., & Dodson, G. G. (1992a) *Biopolymers 32*, 1749−1756.
Smith, G. D., & Dodson, G. G. (1992b) *Proteins: Struct., Funct., Genet. 14*, 401−408.
Smith, G. D., Swenson, D. C., Dodson, E. J., Dodson, G. G., & Reynolds, C. D. (1984) *Proc. Natl. Acad. Sci. U.S.A. 81*, 7093−7097.
Storm, M. C., & Dunn, M. F. (1985) *Biochemistry 24*, 1749−1756.
Sudmeier, J. L., Bell, S. J., Storm, M. C. and Dunn, M. F. (1981) *Science 212*, 560−562.
Whittingham, J. L., Chaudhuri, S., Dodson, E. J., Moody, P. C. E., & Dodson, G. G. (1995) *Biochemistry 34*, 15553−15563.

BI970761N